Laser-induced electron recollision in H_2 and electron correlation

Andre D. Bandrauk* and HuiZhong Lu
Laboratoire de Chimie Théorique, Faculté des Sciences, Université de Sherbrooke, Sherbrooke, Québec, Canada J1K 2R1
(Received 24 January 2005; published 12 August 2005)

Single and double ionization processes are calculated for a 1D model of H_2 from numerical solution of the time-dependent Schrödinger equation in the presence of an intense $I \leqslant 5\times 10^{15}$ W/cm^2, ultrashort (10 cycles) 800 nm laser pulse. Laser-induced electron recollision, LIERC, is identified from a systematic analysis of bound and continuum populations in the two-electron wave function. Recollision is shown to be responsible for double ionization at lower intensities, $I<10^{15}$ W/cm^2 and persists also in the first two excited states of H_2, the $A\ ^3\Sigma_u^+$ and $B\ ^1\Sigma_u^+$ states. The effects of the symmetry (antisymmetry) of the two-electrons wave function is found to be dominant at large internuclear distances where enhanced ionization is operative, especially in the $A\ ^3\Sigma_u^+$, where the exclusion principle suppresses double ionization from LIERC. Furthermore, at large distances, double ionization is shown to occur with equal excitation of the highest occupied and lowest unoccupied molecular orbitals of the H_2^+ core ion. Negligible core excitation occurs at equilibrium.

DOI: 10.1103/PhysRevA.72.023408 PACS number(s): 42.50.Hz

I. INTRODUCTION

Interaction of molecules with intense ($I \geqslant 10^{14}$ W/cm^2) ultrashort ($t<10$ fs) low frequency ($\omega=0.057$ a.u.) or long wavelength (800 nm) laser pulses is a growing area of research [1] due to the availability of laser pulses with variable and controllable amplitudes and phases thanks to steady progress in laser technology [2]. This low frequency regime of laser-matter interaction is characterized by highly nonlinear multiphoton processes at high intensities leading to above threshold ionization (ATI), and high order harmonic generation (HOHG), the latter being the essential source of single attosecond (10^{-18} s) pulses [3,4]. The high intensity low frequency regime can be described by a simple tunnelling ionization process followed by laser-induced electron recollision (LIERC) [5,6], of the ionized electron with the parent ion. It has been applied successfully to explain ATI and HOHG in atoms [2], thus offering a nonlinear nonperturbative theoretical framework based on quasistatic semiclassical ideas [2].

Molecules offer the possibility of the recolliding electron to "diffract" from more than one nuclear center, leading to a phenomenon, laser-induced electron diffraction (LIED) [7], a tool for probing molecular geometry changes on ultrashort time scales [7–9]. Much of the theoretical understanding of LIERC and LIED in molecules is based on solution of the time-dependent Schrödinger equation (TDSE), for the one-electron H_2^+ and H_3^{++} molecules, for static [7,8] and even with moving nuclei [10].

In multielectron atoms, double ionization in intense laser fields has been shown to be a highly correlated process at low intensities with LIERC a dominant mechanism, the nonsequential step [11], transforming to sequential single ionization at higher intensities [12–14]. As indicated in the preceding paragraph, molecules differ from atoms by the multicenter Coulomb nature of any recollision process leading to diffraction. In the present work we shall examine LIERC in a one-dimensional (1D) model of H_2 which we have used previously to examine the effect of electron correlation on HOHG [15]. In particular, at large internuclear distances, tunnelling ionization which is the first step in atomic LIERC, becomes more complicated as a consequence of charge transfer and charge resonance effects, first predicted by Mulliken [16] due to the existence of excited ion-pair states [17] which cross the ground state at high intensities in both 1D [18] and recent three-dimensional (3D) [19] simulation of H_2.

II. TIME-DEPENDENT SCHRÖDINGER EQUATION

The H_2 molecule is the prototype model of the two-electron chemical bond with bonding and antibonding molecular orbitals the essential concepts for understanding the chemical bond [16,20]. Previous 3D calculations of the nonlinear response of H_2 in an intense laser field were performed using a frozen core approximation [21] and time-dependent Hartree-Fock (TDHF) using finite element (FE) methods [22]. Exact 1D [18] and 3D [19] time-dependent Schrödinger equation (TDSE) numerical solutions of H_2 were obtained on large finite grids at equilibrium and large internuclear distances in order to establish the universal molecular phenomenon of charge resonance enhanced ionization (CREI), first discovered in 3D [23] and 1D [24,25] one-electron molecular systems. In the present work we shall investigate LIERC in the first three electronic states of H_2, $X\ ^1\Sigma_g^+$, $A\ ^3\Sigma_u^+$, $B\ ^1\Sigma_u^+$ [20], using exact numerical solutions of the corresponding 1D TDSE [15,18].

The 1D time-independent Born-Oppenheimer (static nuclei) electronic Hamiltonian in atomic units ($e=m=\hbar=1$) can be written for two electrons with coordinates Z_1, Z_2 with respect to the center of mass of two protons situated at positions $\pm R/2$ as

*Electronic address: andre.bandrauk@usherbrooke.ca

$$\hat{H}_0 = -\frac{1}{2}\sum_{i=1}^{2}\left(\frac{\partial^2}{\partial Z_i^2} - \frac{1}{\sqrt{(Z_i \pm R/2)^2 + c}}\right) + \frac{1}{\sqrt{(Z_1 - Z_2)^2 + d}}. \tag{1}$$

The first term in (1) is the kinetic energy, the second term is the electron proton attraction, and the last term is the electron repulsion. The parameters c and d correspond to "softening" parameters removing Coulomb singularities and are used routinely in N-body classical simulations [26] extended to molecules in intense laser fields [27]. In order to obtain numerical solutions of the 1D TDSE mimicking the properties of a 3D H_2, these softening parameters must be chosen judiciously as explained below. The TDSE corresponding to (1) becomes a 2D partial differential equation in the coordinates Z_1, Z_2 and time t for the exact two-electron wave function $\psi(Z_1, Z_2, t)$,

$$i\frac{\partial \psi(Z_1, Z_2, t)}{\partial t} = [\hat{H}_0 + V(Z_1, Z_2, t)]\psi(Z_1, Z_2, t), \tag{2}$$

$$V(Z_1, Z_2, t) = -(Z_1 + Z_2)\mathcal{E}(t)\cos(\omega t). \tag{3}$$

$V(Z_1, Z_2, t)$ is the dipolar (long wavelength) form of the electron-laser interaction for a laser pulse of frequency ω and envelope $\mathcal{E}(t)$. By elimination of the Coulomb singularities in (1) through the softening parameters, c and d, one can use a high order split operator methods [28,29] to propagate the TDSE (2) in time interval $[t, t+\delta t]$ in the two dimensions Z_1, Z_2 from $\psi(Z_1, Z_2, t)$ to the state $\psi(Z_1, Z_2, t+\delta t)$. A third order propagation scheme is generally employed,

$$\psi(t+\delta t) = e^{-i(\delta t/2)W(Z_1,Z_2,t)} e^{i(\delta t/2)[(\partial^2/\partial Z_1)+(\partial^2/\partial Z_2)]} \times e^{-i(\delta t/2)W(Z_1,Z_2,t)}\psi(t), \tag{4}$$

where $W = V(Z_1, Z_2, t) = V(Z_1, Z_2, t+\delta t/2) + V_c(Z_1, Z_2, R)$, i.e., the laser-molecule interaction in (3) plus the Coulomb potentials in (1). We iterate the discrete propagator in (4) to propagate the wave function from some initial electronic bound state $\psi_i(Z_1, Z_2, t=0)$ to the final state $\psi_f(Z_1, Z_2, t=T)$. The final wave function may contain one and two electron continuum states which require a large 2D numerical grid in order to evaluate accurately their occupations and their corresponding probabilities.

The initial states $\psi_i(Z_1, Z_2, 0)$ are obtained from the 1D molecular orbital configurations of the 3D system [20],

$$X\ ^1\Sigma_g^+, \quad \psi_1(Z_1, Z_2) = 1\sigma_g(Z_1)1\sigma_g(Z_2), \tag{5}$$

$$A\ ^3\Sigma_u^+, \quad \psi_2(Z_1, Z_2) = 1\sigma_g(Z_1)1\sigma_u(Z_2) - 1\sigma_u(Z_1)1\sigma_g(Z_2), \tag{6}$$

$$B\ ^1\Sigma_u^+, \quad \psi_3(Z_1, Z_2) = 1\sigma_g(Z_1)1\sigma_u(Z_2) + 1\sigma_u(Z_1)1\sigma_g(Z_2). \tag{7}$$

These satisfy the exclusion principle due to the total spatial-spin antisymmetry of the two particle wave function. Of note is that in both singlet states, electron-electron correlation is strongest, whereas in the triplet state electron recollision should be suppressed due to the antisymmetry of the spatial wave function (6), i.e., $\psi_2(Z_1, Z_2) \to 0$ as $|Z_1 - Z_2| \to 0$. Choosing the orbitals $1\sigma_{g(u)} \simeq [1s_a + (-)1s_b]$, i.e., symmetric (antisymmetric) linear combination of 1D atomic orbitals gives an initial estimate for the initial two-electron wave function. However these are not eigenstates of the discretized zero-field Hamiltonian $\hat{H}_0$ (1). The two-dimensional (2D) eigenstates can be obtained by propagating these initial estimates $(\psi_i, i=1, \ldots, 3)$ in imaginary time using the zero-field TDSE (2,3) and will be used as the initial states of this full TDSE in real time. The imaginary time propagation, which gives the proper initial states $[\psi_i^0(Z_1, Z_2), i=1, \ldots, 3]$ as eigenfunctions of the discretized $\hat{H}_0$ (1), is explored as a function of the softening parameters c/d entering the electron-nuclei attraction and/or electron-electron repulsion in (1), respectively. These parameters are then chosen to give the best possible molecular potentials for the three states studied, X, A, and B of H_2 [30]. We have found the best results with $c=0.7$, $d=1.2375$ giving the three molecular potentials illustrated in Fig. 1. The ground state equilibrium distance is found to be $R_e=1.68$ a.u. and 2.5 a.u. for the B state as compared to 1.4 a.u. and 2.5 a.u. for the 3D molecule. Energy separations at the equilibrium distance $R=1.4$ a.u. are [30] $E(A)-E(X)=0.37$ a.u., $E(B)-E(X)=0.47$ a.u., and $E(X)-E(\infty)=0.17$ a.u., with the last corresponding to the dissociation energy of the ground X state. The corresponding 1D values at $R=1.68$ a.u. with the optimum parameters c and d above are $E(A)-E(X)=0.33$ a.u., $E(B)-E(X)=0.51$ a.u., and $E(X)-E(\infty)=0.17$ a.u.. Clearly the three molecular potentials are adequately represented in our 1D model with parameters c and d in (2). As a further example of the adequacy of the 1D potentials, the force constant $k=\frac{1}{2}(\partial^2 V/\partial R^2)$ for the ground X state is $k_{1D}=0.36$ a.u. whereas $k_{3D}=0.37$ a.u. [30]. Thus for the ground X state both vibrational and dissociation energy are nearly the same in our 1D model and the exact 3D H_2 molecule. We note that in previous 1D simulation of the isoelectronic He atom [14,31,32], both parameters were set at $c=d=1$. As seen from Fig. 1, the 1D model although it reproduces the molecular potentials very well for the first three states of H_2,

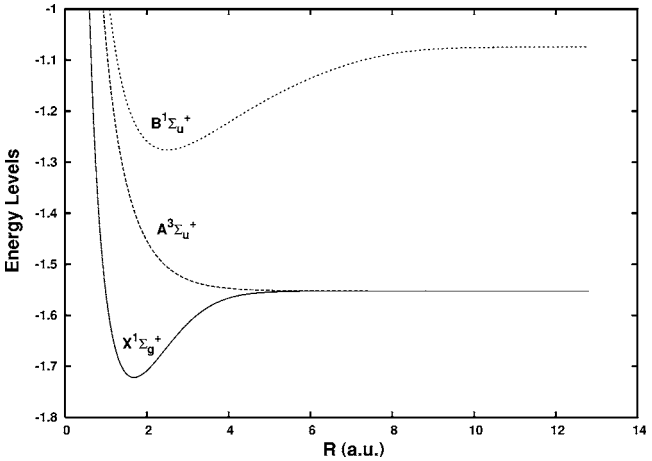

FIG. 1. First three molecular potentials for the 1D H_2 molecule with softened-Coulomb parameter $c=0.7$, $d=1.2375$ [Eq. (1)]. Ground state quilibrium occurs at $R=1.68$ a.u.

nevertheless overestimates the ionization potential by ~0.5 a.u. for all three states, i.e., a constant error, independent of internuclear distance occurs in the 1D model with respect to the 3D system. We nevertheless use this model since the nuclear dynamics which depend on accurate potentials will be the goal of future investigation, as the effect of nuclear motion on molecular ATI and HOHG [10,26].

In order to properly take into account single and double ionization, a large grid with $|Z| \leqslant 1056$ a.u. is used. Spatial integration steps are $\delta Z = 0.4$ a.u. and for time $\delta t = 0.03$ a.u. The convergence of the numerical results are assured by diminishing the temporal/spatial steps and increasing the grid size without changing the obtained results. For analysis, the grid is then separated into three zones for the two electrons, $i = 1, 2$,

$$\text{bound state zone,} \quad \max(|Z_i|) \leqslant 6 \text{ a.u.},$$

$$\text{single electron ionized zone,} \quad \min(|Z_i|) \leqslant 6 \text{ a.u.},$$

$$\max(|Z_i|) > 6 \text{ a.u.},$$

$$\text{double electrons ionized zone,} \quad \min(|Z_i|) > 6 \text{ a.u.}$$

As an example we show the time evolution $\psi_1(Z_1, Z_2, t)$ for the ground X state (5) after two cycles [Fig. 2(a)] and six cycles [Fig. 2(b)] at equilibrium $R = 1.68$ a.u. for an intensity $I = 3 \times 10^{15}$ W/cm^2 at $\lambda = 800$ nm. One sees clearly that initially [Fig. 2(a)] one electron is exiting along the axis Z_1, $Z_2, \simeq 0$ with the width of the wave packet representing essentially the dimension of the remaining bound states. After six cycles, the double ionization regions begin to fill up [Fig. 2(b)]. The delineation between bound and continuum states becomes more difficult as seen by the expansion of the bound states via Rydberg states in Fig. 2(b). Thus integration of probabilities in the bound state zone [$\max(|Z_i|) \leqslant 6$ a.u.] as real bound states need to be verified. We follow here the procedure of Pindzola *et al.* [32], of projection of the total final wave function $\psi_f(Z_1, Z_2, t = T)$ on complete sets of field free bound and continuum states of the 1D one-electron H_2^+ ion obtained from the same numerical grid. The probability of finding one electron in the bound state $\psi_m(Z_1)$ and the second in bound state $\psi_n(Z_2)$ is calculated as

$$P_{mn}(t) = |\langle \psi_m(Z_1)\psi_n(Z_2)|\psi(Z_1, Z_2, t)\rangle|^2. \tag{8}$$

So the total bound state occupation is given by $P_b(t) = \Sigma_{mn} P_{mn}(t)$. Similarly the probability of finding one electron in bound state ψ_n and the other electron in the continuum state is

$$P_{nk}(t) = 2 \int dZ_1 |\langle \psi_n(Z_2)|\psi(Z_1, Z_2, t)\rangle|^2 - \sum_m P_{mn}(t). \tag{9}$$

$P_1 = \Sigma_n P_{nk}$ gives therfore the single ionization probability. Finally the probability of double ionization can be calculated by

$$P_2(t) = P_{kk}(t) = 1 - \sum_n P_{nk}(t) - P_b(t). \tag{10}$$

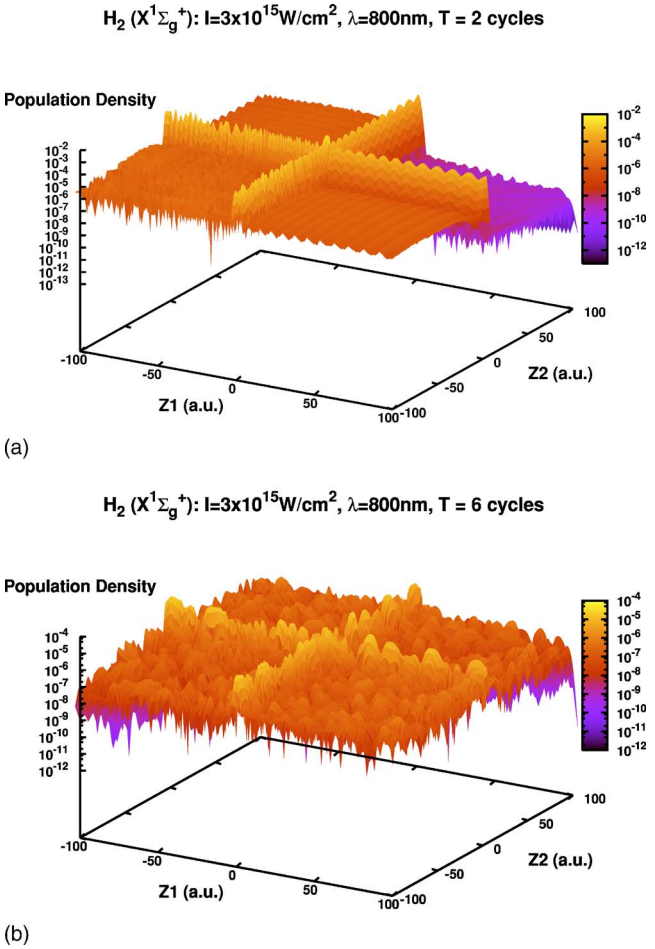

FIG. 2. (Color online) 2D ground state electron density $|\psi_X(Z_1, Z_2, t)|^2$ at $R = 1.68$ a.u. for intensity $I = 3 \times 10^{15}$ W/cm^2, $\lambda = 800$ nm: (a) $t = 2$ cycles; (b) 6 cycles (1 cycle = 1.87 fs).

III. LIERC AT EQUILIBRIUM

Solution of the two-electron TDSE, Eqs. (3) and (4), gives the exact 1D two particle wave function $\psi(Z_1, Z_2, t)$. By numerical integration of the probability density $|\psi(Z_1, Z_2, t)|^2$ over different regions of the 2D grid decomposition defined in the preceding section allows for identification of the following probabilities: bound state probability P_b is the integration over the bound state zone, single ionization probability P_1 is the integration over the single electron ionized zone, and double ionization P_2 is given by the integration over the double electron ionized zone. These are to be compared to populations obtained by projection of the two particles wave function $\psi(Z_1, Z_2, t)$ onto numerical single particle wave function of H_2^+, and defined in Eqs. (8)–(10). We illustrate these results in Fig. 3 for the initial $1\sigma_g^2$ configuration of the ground $X\ ^1\Sigma_g^+$ state at the equilibrium distance $R = 1.68$ a.u. Comparing Figs. 3(a) and 3(b) shows that the direct integration and projection methods agree very well, thus justifying the definition of $|Z| \leqslant 6$ a.u. as the bound state region in the direct integration method. Both Figs. 3(a) and 3(b) show a distinct "knee" in P_2 as the single ionization P_1 saturates to its maximum at 1 around 10^{15} W/cm^2. Figure 3(b) shows the onset of a ionization regime at the end of the knee around

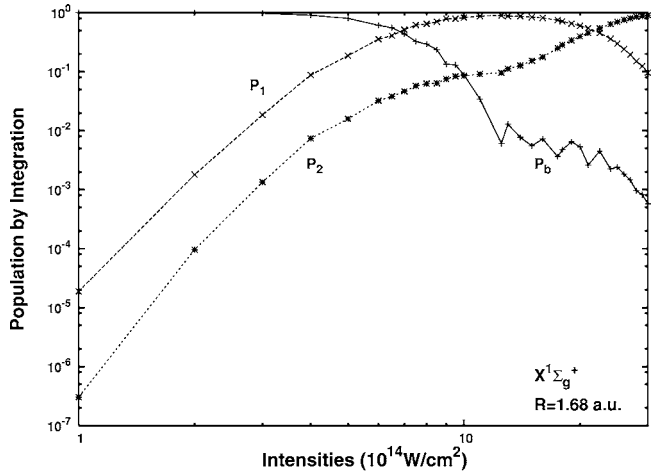

(a)

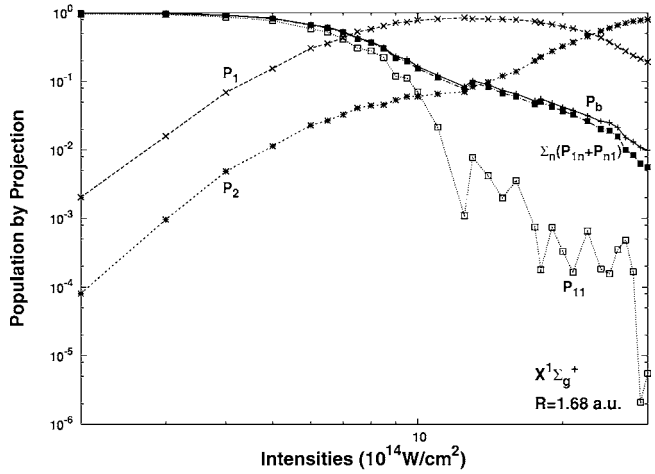

(b)

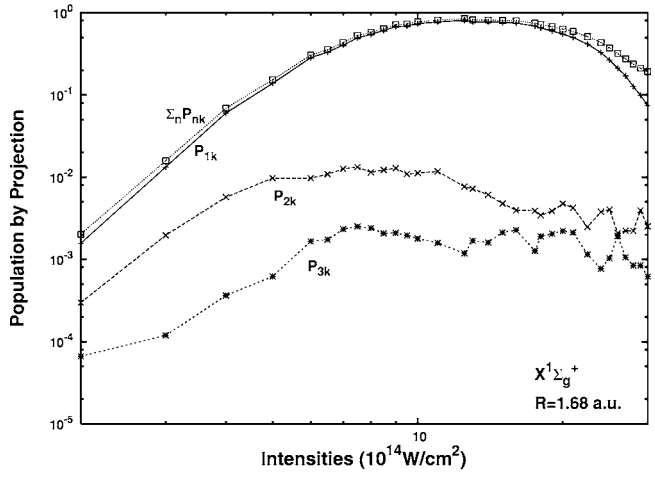

(c)

FIG. 3. (a) Single ionization P_1, double ionization P_2, and bound state P_b probabilities for initial ground state $X\ ^1\Sigma_g^+$ as a function of intensity obtained by numerical integration at $R=1.68$ a.u. (b) P_1, P_2, P_b obtained by projection onto eigenstates of H_2^+; P_{11} and $\Sigma_n P_{1n}+P_{n1}$ are probabilities of no bound state excitation, and single excitation to bound state n, respectively. (c) Bound state (n) to continuum (k) probabilities P_{nk} and total sum $\Sigma_n P_{nk}$ [Eq. (10)].

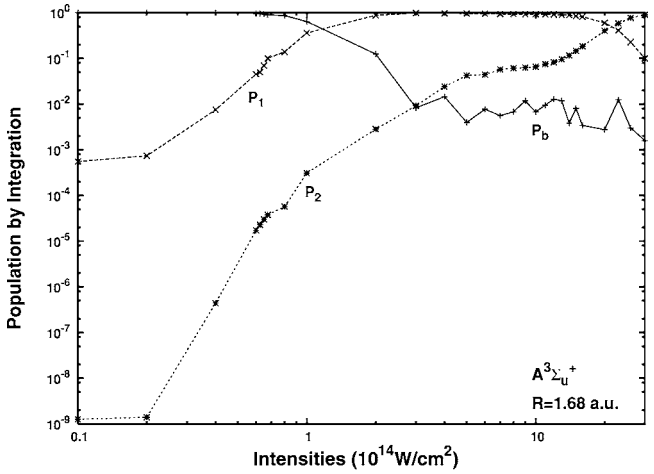

(a)

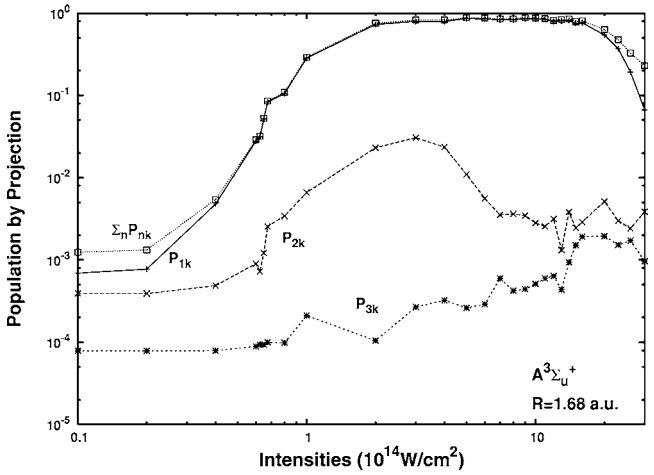

(b)

FIG. 4. (a) Single ionization P_1, double ionization P_2, and bound state P_b probabilities for initial excited state $A\ ^3\Sigma_u^+$ as a function of intensity at $R=1.68$ a.u. (b) Bound state (n) to continuum (k) probabilities P_{nk} and then total sum $\Sigma_n P_{nk}$.

10^{15} W/cm^2 corresponds to a sharp decrease of P_{11}, the probability of finding the two electrons in the ground state. Figure 3(c) illustrates the various excitation probabilities of the remaining bound electron in the single ionization. Very little excitation of the remaining H_2^+ core is obtained. Both Figs. 3(a) and 3(b) show that single (P_1) and double (P_2) ionization are parallel below the intensity 10^{15} W/cm^2, thus indicating P_2 is proportional to P_1. The knee in P_2 around 10^{15} W/cm^2 is followed at high intensities by an increase in P_2 with a different slope and a depletion of the bound state P_b, indicative of complete ionization. We conclude from Fig. 3 that two different ionization mechanisms exist. At intensities $I<10^{15}$ W/cm^2, double ionization is directly proportional to the single ionization probability with saturations of both at the same intensity. At high intensity, double ionization is independent of single ionization and correlates as expected with complete depletion of bound states. Little excitation of the core of H_2^+ is obtained, since the excited states of the latter are of much larger energy than the 800 nm photon energies.

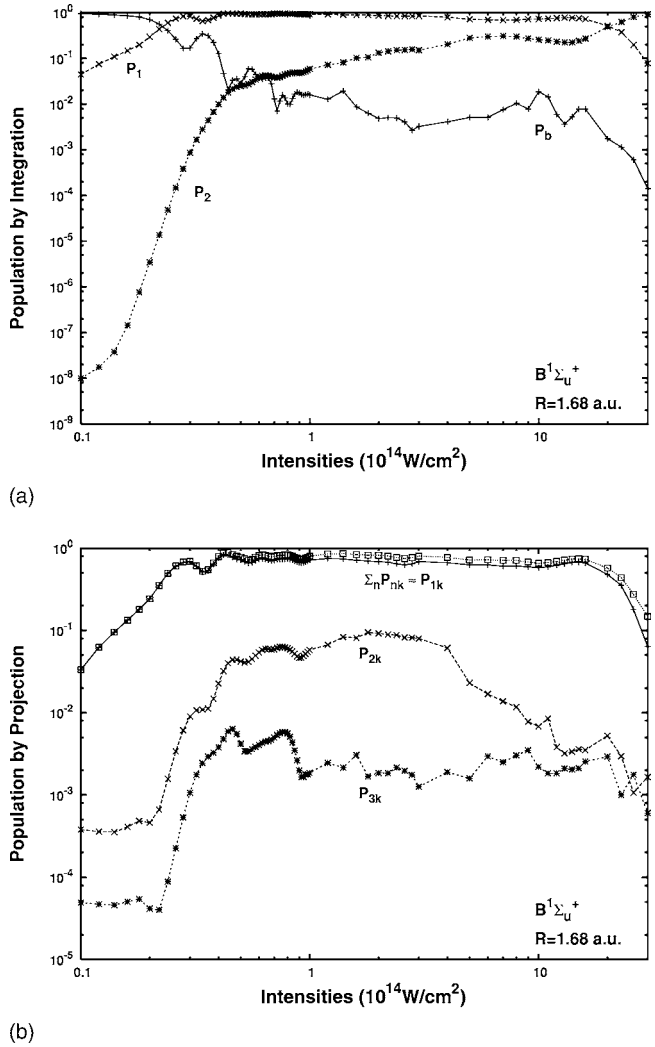

FIG. 5. (a) Single ionization P_1, double ionization P_2, and bound state P_b probabilities for initial excited state $B\ ^1\Sigma_u^+$ as a function of intensity at $R=1.68$ a.u. (b) Bound state (n) to continuum (k) probabilities P_{nk} and then total sum $\Sigma_n P_{nk}$.

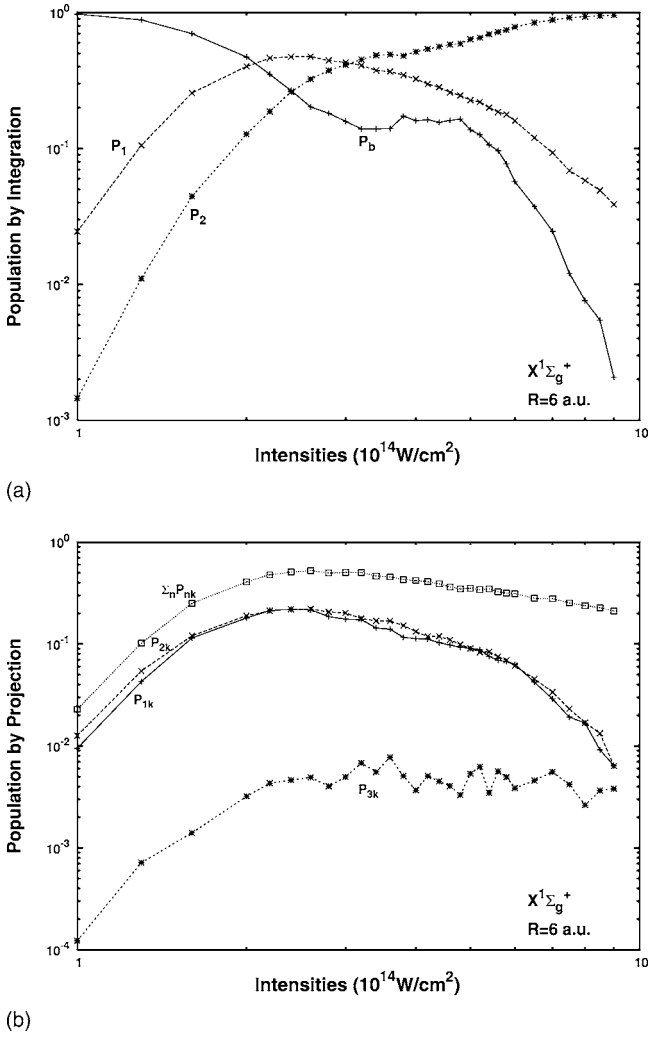

FIG. 6. (a) Single ionization P_1, double ionization P_2, and bound state P_b probabilities for initial ground state $X\ ^1\Sigma_g^+$ as a function of intensity at $R=6$ a.u. (b) Bound state (n) to continuum (k) probabilities P_{nk} and then total sum $\Sigma_n P_{nk}$.

In Fig. 3 we examined single and double ionization of the $1\sigma_g^2$ configuration of the ground $X\ ^1\Sigma_g^+$ state of H_2. In the Hartree-Fock (HF) approximation due to the Pauli exclusion principle, there is no exchange energy in zero field, i.e., the orbitals are solutions of Hartree equations with electron-electron repulsion the only correlation mechanism. We now turn our attention to the next two excited states, the triplet A state and the singlet B state. As seen from Eqs. (5)–(7), these states involve exchange of electrons between orbitals of different symmetry, $1\sigma_g$ and $1\sigma_u$. Thus in addition to electron repulsion, exchange energies are now negative in the A state and positive in the B state, i.e., electron repulsion will be minimum in the triplet A state and maximum in the singlet B state [20]. We compare therefore the ionization of each in Figs. 4 and 5, respectively, where only population obtained by numerical integration are reported as projection population as described above for the ground state were nearly identical. The main difference in the ionization of both states occurs in the double ionization P_2. The double knee for the B state has become a plateau extending from intensity 5 $\times 10^{14}$ W/cm^2 up to 2×10^{15} W/cm^2 whereas in the A state the double ionization knee is much less pronounced. We interpret this as the influence of the exclusion principle in this state which suppresses the double electron probability, i.e., $|\psi(Z_1,Z_2,t)|^2 \to 0$ for $|Z_1-Z_2| \to 0$. Thus in this triplet state recollision is diminished whereas in the B state it is enhanced. One must keep in mind that the single ionization probability is larger in the B state as seen in Fig. 5(a) where the bound state probability P_b decreases already at lower intensities than in the A state, Fig. 4(a). Thus both larger single ionization P_1 and larger electron correlation are seen to operate in the B state. Finally both Fig. 4(b) and Fig. 5(b) show little excitation of the H_2^+ $(1\sigma_g)$ core, showing that it is indeed the antibonding $1\sigma_u$ electron which is the first to ionize.

IV. LIERC AT LARGE INTERNUCLEAR DISTANCE

Molecules differ from atoms due to the possibility of charge transfer induced by intense fields, leading to en-

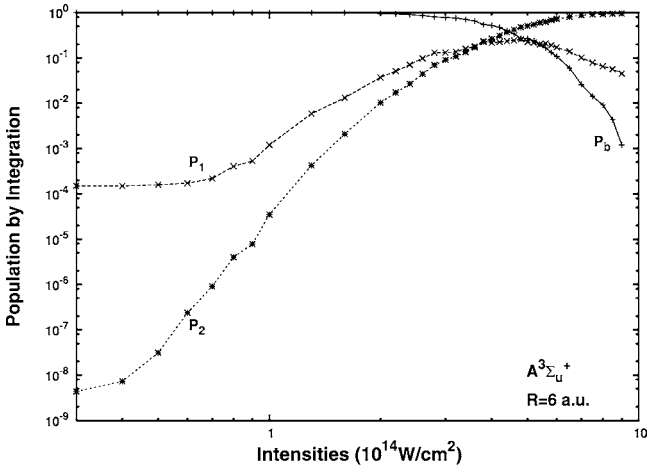

FIG. 7. (a) Single ionization P_1, double ionization P_2, and bound state P_b probabilities for initial excited state $A\ ^3\Sigma_u^+$ as a function of intensity at $R=6$ a.u. (b) Bound state (n) to continuum (k) probabilities P_{nk} and then total sum $\Sigma_n P_{nk}$.

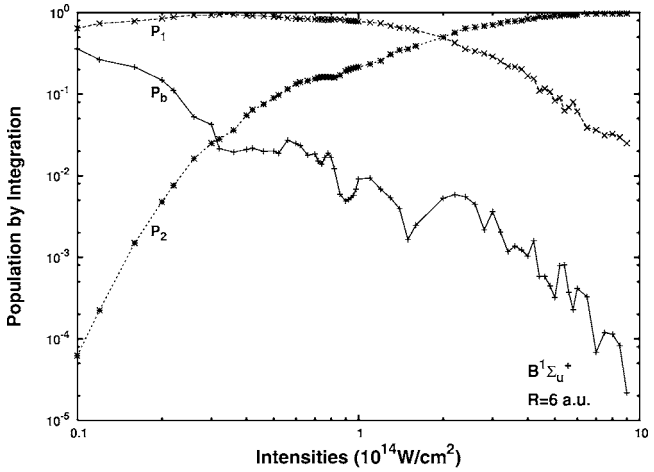

FIG. 8. (a) Single ionization P_1, double ionization P_2, and bound state P_b probabilities for initial excited state $B\ ^1\Sigma_u^+$ as a function of intensity at $R=6$ a.u. (b) Bound state (n) to continuum (k) probabilities P_{nk} and then total sum $\Sigma_n P_{nk}$.

hanced ionization at critical internuclear distances [1,23–25]. In the case of the two-electron system H_2, and linear H_3^+ [18], a quasistatic model where one assumes ionization occurs mainly at the peak of the field $\mathcal{E}$, predicts such enhanced ionization occurs around $R_C \simeq 6$ a.u. We therefore examine single and double ionization of our 1D H_2 at that internuclear distance. As shown earlier, extended molecular systems are subject to strong electron correlation with the result that much longer HOHG plateaus are obtained due to electron-electron energy exchange [15]. Furthermore, at this distance, the electronic orbitals $1\sigma_g$ and $1\sigma_u$ of H_2^+ become nearly degenerate, resulting in near equal population of both for laser frequencies larger than their energy separation [15,23,33]. This equalization of population of the highest occupied [HOMO($1\sigma_g$)] and lowest unoccupied [LUMO($1\sigma_u$)] molecular orbitals of H_2^+ is responsible for charge resonance enhanced ionization (CREI) in H_2^+ and odd electron molecules in general [1].

We illustrate in Figs. 6–8, the single, double ionization, and bound state probabilities and the single excitation population for the three electronic states, X, A, and B, respectively, at $R=6$ a.u. as a function of intensity from 10^{14} to 10^{15} W/cm^2. In both single states X and B, Figs. 6(a) and 8(a), we find a knee (plateau) in the double ionization P_2. No such knee occurs in the triplet A state, Fig. 7(a). For all three electronic states, perusal of Figs. 6(b), 7(b), and 8(b) show that during single ionization, both $1\sigma_g$ and $1\sigma_u$ orbitals of the H_2^+ core are nearly always equally populated during the ionization. Thus double ionization at the CREI distance R_c occurs as a coherent process with ejection of the second electron from two coherently coupled orbitals, $1\sigma_g$ and $1\sigma_u$. This striking effect does not occur at equilibrium distance where these two orbitals are well separated in energy, much larger than the single photon (laser) energy (Figs. 3–5).

The seemingly effective suppression of electron recollision effects, in the A state reflects the difference in the electronic structure at large distances of the ground X and first excited A states. These are known to correlate asymptotically to the Heither-London or valence-bond states [20],

$$\psi_{X(A)}(Z_1,Z_2,0) \rightarrow 1s_a(1)1s_b(2) + (-)1s_a(2)1s_b(1). \quad (11)$$

Thus electron correlation transforms delocalized molecular orbitals $1\sigma_{g(u)}$ into localized atomic orbitals $1S_{a(b)}$ on atom $a(b)$. Ionization will occur from either atom at large distance. Double ionization at large distances by recollision requires both electrons to be at the same atom which is prohibited by the exclusion principle in the triplet A state. Alternatively, one can see from the A state wave function (6), any transformation of $1\sigma_g$ into $1\sigma_u$ and vice versa reduces the wave function and thus its probability by virtue of the antisymmetry inherent in that wave function. The equal occupation of $1\sigma_g$ and $1\sigma_u$ orbitals is the signature of field induced localization of electrons in each atom and concomitant CREI [23,33]. We conclude from this study that at large internuclear distances, Pauli exclusion effects dominates in LIERC and that the ion core of odd electron systems undergo field induced electron localization so that double ionization occurs coherently from simultaneously occupied molecular orbitals.

V. CONCLUSION

Laser induced electron recollision, a fundamental concept used to rationalize atom multiphoton ionization with intense low frequency laser pulses has been identified from numerical solutions of the TDSE for a 1D model of H_2. The recollision process has been shown to occur in the ground state X and the first two excited states of H_2, A and B. Both X and B states, being singlet electronic states show strong correlation effects as compared to the triplet A state where the Pauli exclusion principle diminishes such effects. Negligible excitation of the core of the H_2^+ ion is found during the single ionization process at the equilibrium distance of the molecule.

At larger internuclear distances, equal excitation of the HOMO ($1\sigma_g$) and LUMO ($1\sigma_u$) of the H_2^+ core is found during the first ionization. This leads to electron localization and enhanced ionization of both the H_2 and the ion core H_2^+. Enhanced LIERC is found in the singlet B state and suppression in the triplet A state, thus reflecting the dominance of electron correlation upon dissociation of the molecule and its importance in electron-molecule recollision processes.

ACKNOWLEDGMENTS

The authors thank their colleagues P.B. Corkum and S. Chelkowski for "illuminating" discussions on electron recollision. The authors also acknowledge use of SGI and IBM parallel supercomputers operated by RQCHP (Reseau Quebecois de Calcul de Haute Performance).

[1] A. D. Bandrauk and H. Kono, in *Advances in Multiphoton Processes and Spectroscopy*, edited by S. H. Lin, A. A. Villaeys, and Y. Fujimura (World Scientific, Singapore, 2003), Vol. 15, pp. 154–212.
[2] T. Brabec and F. Krausz, Rev. Mod. Phys. **72**, 545 (2000).
[3] M. Hentschel *et al.*, Nature (London) **414**, 509 (2001).
[4] A. D. Bandrauk and H. S. Nguyen, Phys. Rev. A **66**, 031401(R) (2002).
[5] P. B. Corkum, Phys. Rev. Lett. **71**, 1994 (1993).
[6] K. J. Schafer, B. Yang, L. F. Di Mauro, and K. C. Kulander, Phys. Rev. Lett. **70**, 1599 (1993).
[7] T. Zuo, A. D. Bandrauk, and P. B. Corkum, Chem. Phys. Lett. **259**, 313 (1996).
[8] A. D. Bandrauk and S. Chelkowski, Phys. Rev. Lett. **87**, 273004 (2001).
[9] J. Hatani *et al.*, Nature (London) **432**, 867 (2004).
[10] A. D. Bandrauk, S. Chelkowski, and I. Kawata, Phys. Rev. A **67**, 013407 (2003).
[11] G. L. Yudin and M. Y. Ivanov, Phys. Rev. A **63**, 033404 (2001).
[12] B. Walker, B. Sheehy, L. F. Di Mauro, P. Agostini, K. J. Schafer, and K. C. Kulander, Phys. Rev. Lett. **73**, 1227 (1994).
[13] X. Liu *et al.*, Phys. Rev. Lett. **93**, 263001 (2004).
[14] N. E. Dahlen and R. van Leuwen, Phys. Rev. A **64**, 023405 (2001).
[15] A. D. Bandrauk and H. Yu, Phys. Rev. A **59**, 539 (1999).
[16] R. S. Mulliken, J. Chem. Phys. **7**, 20 (1939).
[17] J. D. D. Martin and J. W. Hepburn, Phys. Rev. Lett. **79**, 3154 (1997).
[18] I. Kawata, H. Kono, and A. D. Bandrauk, Phys. Rev. A **64**, 043411 (2001).
[19] K. Harumiya, H. Kono, Y. Fujimura, I. Kawata, and A. D. Bandrauk, Phys. Rev. A **66**, 043403 (2002).
[20] J. C. Slater, *Quantum Theory of Molecules and Solids* (McGraw-Hill, New York, 1963), Vol. 1.
[21] J. L. Krause, K. J. Schafer, and K. C. Kulander, Chem. Phys. Lett. **178**, 573 (1991).
[22] H. Yu and A. D. Bandrauk, J. Chem. Phys. **102**, 1257 (1995).
[23] T. Zuo and A. D. Bandrauk, Phys. Rev. A **52**, R2511 (1995); **54**, 3254 (1996).
[24] S. Chelkowski and A. D. Bandrauk, J. Phys. B **28**, L723 (1995).
[25] T. Seideman, M. Y. Ivanov, and P. B. Corkum, Phys. Rev. Lett. **75**, 2819 (1995).
[26] J. U. Brackbill and B. I. Cohen, *Multiple Time Scales* (Academic, Orlando, 1985).
[27] D. M. Villeneuve, M. Y. Ivanov, and P. B. Corkum, Phys. Rev. A **54**, 736 (1996).
[28] A. D. Bandrauk and H. Shen, J. Chem. Phys. **99**, 1185 (1993); J. Phys. A **27**, 7147 (1994).
[29] S. Chelkowski, C. Foisy, and A. D. Bandrauk, Phys. Rev. A **57**, 1176 (1997).
[30] W. Kolos and L. Wolniewicz, J. Chem. Phys. **43**, 2429 (1965); **45**, 509 (1966).
[31] D. G. Lappas and R. Van Leuwen, J. Phys. B **31**, L249 (1998).
[32] M. S. Pindzola, F. Robicheaux, and P. Gavras, Phys. Rev. A **55**, 1307 (1997).
[33] T. Zuo, S. Chelkowski, and A. D. Bandrauk, Phys. Rev. A **49**, 3943 (1994).